Journal of Power Sources 250 (2014) 160–165

Contents lists available at ScienceDirect

Journal of Power Sources

journal homepage: www.elsevier.com/locate/jpowsour

Short communication

# Growth of Si nanowires in porous carbon with enhanced cycling stability for Li-ion storage

Xiaoxu Zhao, Xianhong Rui, WenWen Zhou, Liping Tan, Qingyu Yan, Ziyang Lu*, Huey Hoon Hng*

*School of Materials Science and Engineering, Nanyang Technological University, 50 Nanyang Avenue, Singapore 639798, Singapore*

## HIGHLIGHTS

- Solution-liquid–solid growth of Si nanowires in porous carbon.
- Porous carbon improve electrical conductivity and buffer volume change.
- Synergistic effect between porous carbon and Si nanowires enhances capacities.
- High reversible capacity of 1678 mAh $g^{-1}$ during the 100th cycle at a current density of 420 mA $g^{-1}$.

## ARTICLE INFO

*Article history:*
Received 20 September 2013
Received in revised form
6 November 2013
Accepted 8 November 2013
Available online 18 November 2013

*Keywords:*
Lithium ion battery
Porous carbon
Silicon nanowires
Anode

## ABSTRACT

Si nanowires are successfully grown in porous carbon by supercritical fluid-liquid-solid (SFLS) process, which show high specific capacities and charge–discharge cycling stability as anode materials for Li-ion storage. The enhancement capacity and cycling stability of the Si nanowires/porous carbon composite nanostructures is attributed to the porous carbon serving as a highly conductive framework and absorption of volume changes of Si nanowires during the lithiation/delithiation process. At optimized condition, the Si nanowires/porous carbon electrodes maintain reversible capacities of 1678 mAh $g^{-1}$ for the 100th cycle at a current density of 420 mA $g^{-1}$, which is much better as compared to that of pure Si nanowires.



## 1. Introduction

During the past decades, great efforts have been devoted to the preparation of new electrode with high capacity and good stability for lithium-ion battery due to its wide applications in portable electronics [1–5]. Among the various candidate materials for anode electrode, silicon has received extensive attention due to its highest known theoretical capacity (4200 mAh $g^{-1}$ for $Li_{22}Si_5$) and abundance [6–10]. However, the large volume change (360%) during the discharge-charge reactions cause the loss of contact between silicon and the current collection, which leads to fast capacity fading with increasing cycles [11]. To overcome this problem, researchers have developed many silicon nanostructures as lithium-ion battery anode materials such as nanoparticles, nest-like nanospheres, nanotube, nanosheets and nanowires [3,10,12–16]. The advantage of using Si nanowires instead of other morphologies is that it provides good electrical conductivity along the length of individual nanowires, short lithium ion diffusion distance and large interfacial area in contact with the electrolyte [10,17–19].

Recently, it was found that the stability of silicon electrode can be further enhanced by combining the nanostructures silicon with carbon material as a result of increased electrical conductivity, aggregation prevention and buffering volume changes [20–28]. For examples, silicon nanoparticles and nanowires coated with a thin carbon film [10,23] showed improved cycling stability. Combination of silicon with carbon nanotube or graphene displays high electrical conductivity which contributes the high cycling stability of the electrode [26,29]. Dispersing silicon nanoparticles in porous carbon matrix is also a good way to achieve high capacity and good stability. For instance, Magasinski et al. designed a chemical vapor deposition (CVD) synthesis process for robust porous carbon spheres loading with silicon nanoparticles as high-performance lithium-ion battery anodes [30].

In this paper, we report for the first time the solution growth of silicon nanowires in porous carbon (Si NWs/PC). The weight ratio of

* Corresponding authors. Tel.: +65 6790 4140; fax: +65 6790 9081.
*E-mail addresses:* zylu@ntu.edu.sg (Z. Lu), ashhhng@ntu.edu.sg (H.H. Hng).

0378-7753/$ – see front matter © 2013 Elsevier B.V. All rights reserved.
http://dx.doi.org/10.1016/j.jpowsour.2013.11.008

the Si NWs can be easily adjusted by changing the precursor ratio during the preparation. As anode materials for Li-ion storage, these materials showed improved specific capacities and charge–discharge cycling stability (e.g. delivering a reversible capacity of 1678 mAh $g^{-1}$ during the 100th cycle at 0.1 C) as compared to that of pure Si NWs because the porous carbon provides better electronic pathways and also acts as a buffering phase for the volume changes of Si.

## 2. Experimental

### 2.1. Preparation of pure silicon nanowires

In a typical Si NWs synthesis, 0.1 mL of diphenylsilane (DPS) and Au seeds in the molar ratio of Au:Si being 1:150, were added to 20 mL of hexane in a glass beaker. The beaker was then placed in a high pressure high temperature (HPHT) reactor (Model: 4576, Parr Instrument Company), purged with argon gas for 10 min and then sealed up. The reaction mixture was heated in the reactor to 360 °C at a rate of about 10 °C $min^{-1}$ and stand for 2 h. After cooling down, the as-synthesized Si NWs were rinsed with hexane and annealed at 650 °C in a tube furnace with Ar protection.

### 2.2. Growth of silicon nanowires in porous carbon

The synthesis of Si NWs in porous carbon is illustrated in Fig. 1. Firstly, gold seeds were prepared in porous carbon. Typically, 100 mg porous carbon (Vulcon XC 72) and 2 mL of 5 mM $HAuCl_4$ were mixed in 10 mL water. After 2 h, 1 mL of 0.1 M $NaBH_4$ was added and reacted for 1 h. The porous carbon–gold composite was separated by centrifugation and dried in vacuum oven. Si NWs were synthesized by thermally degrading diphenylsilane (DPS) in hexane at 360 °C. The gold/porous composite was put into the reactor, and then 20 ml hexane and diphenylsilane (with different amount) were added. The temperature was increased to 360 °C by the rate of 10 °C $min^{-1}$ and stand for 2 h. After cooling down, the sample was rinsed with hexane and annealed at 650 °C in a tube furnace with Ar protection.

### 2.3. Characterization

Transmission electron microscopic (TEM) observations were carried out under a JEOL-2010 electron microscope after the dilute dispersions of the particles were dropped onto carbon coated copper grids. The morphologies of the composites were investigated by using a JEOL JEM-7600F field emission scanning electron microscope (FESEM). X-ray diffraction (XRD) patterns were acquired on a Shimadzu X-ray diffractometer (Cu Kα). Electrochemical experiments were performed by assembling two-electrode coin cells in an argon-filled glove box with Li foil as the counter electrode and 1 M $LiPF_6$ in EC/DEC as the electrolyte. For Si NWs/PC, the electrodes were prepared by mixing 90 wt% of the active materials and 10 wt% of poly(vinylidene fluoride) binder and then coating on copper foil. For pure Si NWs, the electrodes were prepared by mixing 80 wt% of the active materials 10% super P carbon black and 10 wt% of poly(vinylidene fluoride) binder and then coated on copper foil. The obtained electrodes were dried under vacuum at 50 °C for 12 h. The cells were charged and discharged within the voltage window from 0.005 to 1.5 V. Cyclic voltammetry and electrochemical impedance spectroscopy (EIS, frequency range: 0.001–$10^5$ Hz, amplitude: 5 mV) analysis were performed with an electrochemical workstation (CHI 660C).

## 3. Results and discussion

### 3.1. Structure and morphology

The typical sample preparation process is described in the scheme displayed in Fig. 1. Gold nanoparticles were firstly embedded in porous carbon matrix, which is confirmed by TEM and HRTEM images (Fig. 2). The particles size is typically in the range of 10 nm–20 nm with polycrystalline phase. These gold nanoparticles served as seeds for the further growth of Si NWs by supercritical fluid-liquid-solid process (SFLS) [31]. During the SFLS process, the precursor (DPS) was decomposed into silicon atom and then dissolving into the melting gold seeds. As more Si dissolves, the gold droplets become saturated and expel Si in the form of crystalline nanowires. After the reaction, the Si NWs grow in porous carbon while the hexane solutions remain clear. Fig. 3 shows TEM and FESEM images of the Si NWs/PC composite. A large quantity of nanowires was obtained. Although it is hard to clearly observe all the Si NWs in porous carbon in the TEM image (Fig. 3a) due to the three dimensional structure, the magnified TEM image (Fig. 3c) of a single Si NW shows the Si NW is surrounded with carbon. It can be seen clearly from the FESEM images (Fig. 3b) that the Si NWs are embedded in the porous carbon with diameters of 30–70 nm, which is much smaller than the Si NWs prepared by etching Si wafer [32]. The diameter of the Si NWs is larger and broader than that of the gold seeds which is due to the aggregation of the seeds during the SFLS process [31]. The lattice fringes of the Si NW in porous carbon are also observed in the HRTEM image in Fig. 3d, which shows d-spacing of 3.12 Å, corresponding to the (111) plane. And the XRD patterns (Fig. 4) of Si NWs/PC show the signature peaks of cubic Si (JCPDF 89-5012). In addition, diffraction peaks corresponding to the (111) plane of the cubic gold phase (JCPDF 89-3697) and copper (JCPDF 89-2838) were also observed, which are from the gold seeds and Cu substrate. The Cu substrate serves as the current collector for the electrochemical measurements.

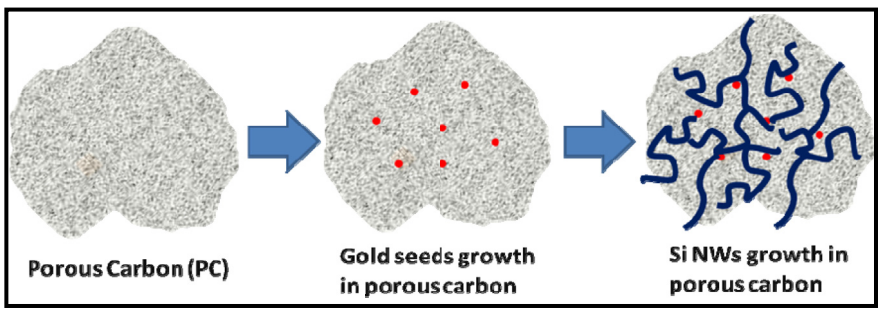


**Fig. 1.** Schematic illustration of the synthetic process of Si NWs/Porous carbon composite. Gold seeds were embedded in the porous carbon, and then the silicon nanowires were grown in the porous carbon by supercritical fluid-liquid-solid (SFLS) process.

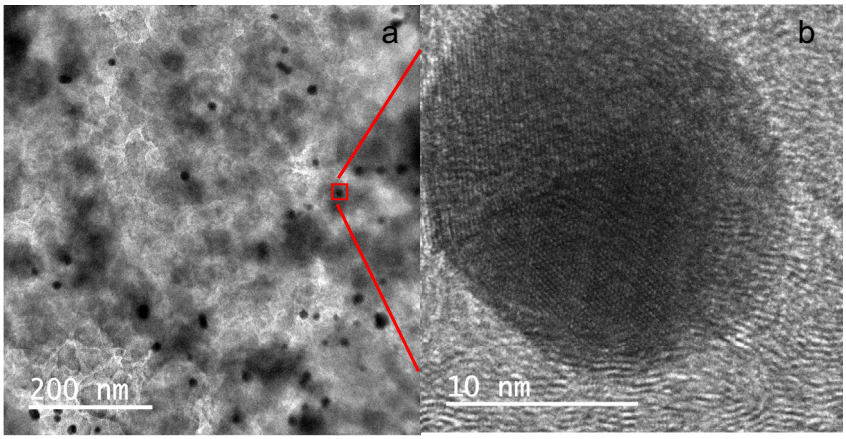


**Fig. 2.** (a) TEM image and (b) HRTEM image of porous carbon decorated with gold nanoparticles.

The percentage of Si NWs in the composite can be changed by adjusting the precursor concentration. Fig. 5 shows the FESEM images of pure Si NWs and Si NWs/PC composite with different amount of Si NWs. The pure Si NWs are generally smooth with diameters in the range of 30–70 nm and a length of >10 μm. However, Si NWs in porous carbon are usually tortuous because the pores in carbon are irregular which confine the growth of the Si NWs. Part of the Si NWs is extended out of the porous carbon. When more silicon precursor was used, more Si NWs were exposed. The amount of the Si NWs in the composite was estimated with gravimetric method after calcinations in air at 800 °C for 4 h to convert all the Si into $SiO_2$ [30]. The percentage of the three Si NWs/PC samples was calculated to be 54.5%, 71.4 and 80% respectively.

### 3.2. Electrochemical measurements

A series of electrochemical measurements were carried out to study the Li-ion storage capabilities of the Si NWs/PC composites based on the half-cell configuration. Fig. 6a shows the initial charge-discharge voltage profiles of the pure Si NWs and Si NWs/PC

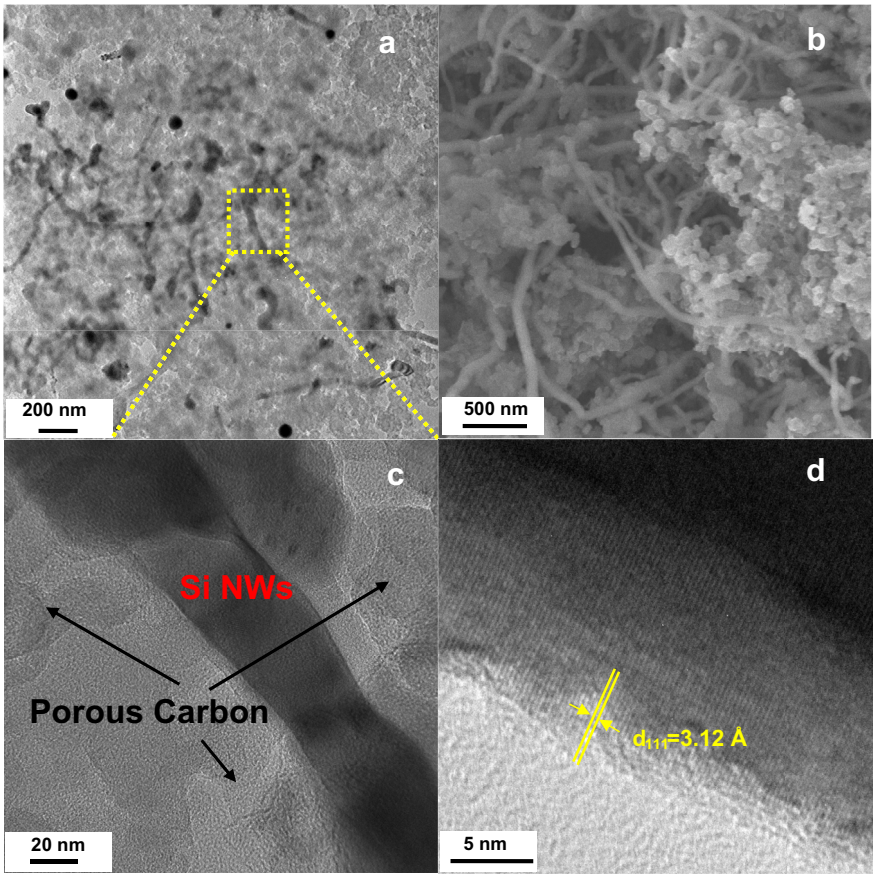


**Fig. 3.** (a, c) TEM image, (b) SEM image and (d) HRTEM image of silicon nanowire in porous carbon.

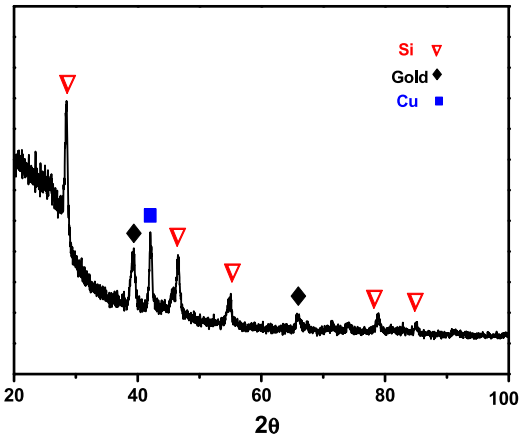


**Fig. 4.** XRD of silicon nanowires/porous carbon composite.

composites electrodes at a current density of 420 mA $g^{-1}$ (0.1 C). The potential plateaus observed in the discharge curves were consistent with previous reports, which correspond to the following electrochemical reactions [33,34]:

Si (crystal) → $Li_xSi$ (amorphous) → $Li_{15}Si_4$ (crystal) ↔ Si (amorphous)

The observed plateau at 0.6 V is associated with the formation of solid–electrolyte interface (SEI) film [35] due to the reduction of electrolyte. For the pure Si NW electrode, the insertion process gave an initial discharge capacity of 4079 mAh $g^{-1}$ and a subsequent charge capacity of 2363 mAh $g^{-1}$, resulting in a Coulombic efficiency of 57.9%. However, when the Si NWs were embedded in porous carbon matrix, the Coulombic efficiency for the first cycle increased significantly. For example, the initial discharge capacity of Si NWs/PC composites with 80%, 71.4% and 54.5% Si NWs are 3398, 2863 and 2204 mAh $g^{-1}$ respectively, and the first charge capacity are 2469, 2130 and 1756 mAh $g^{-1}$, giving Coulombic efficiency of 72.6%, 74.4% and 79.6%. Here, it should be noted that the capacity value is calculated based on the mass of Si/C composite. These results prove the addition of the carbonaceous phase can increase the first cycle Coulombic efficiency. The irreversible capacity losses in the first cycle may be attributed to the losing in electronic contact after the initial volume change. As the porous carbon improves the resiliency of the electrode and buffer the volume changes effectively, the larger amount of porous carbon used, the higher the first cycle Coulombic efficiency can be obtained.

The discharge-charge cycling performances of the Si NWs and Si NWs/PC electrodes were evaluated at 0.1 C (Fig. 6b), and the discharge capacity for first three cycles are shown in the inset for clarity. The Si NWs showed a high initial discharge capacity of 4079 mAh $g^{-1}$, which decreased rapidly to 1975 mAh $g^{-1}$ at the second cycle, and then fast fading to 316 mAh $g^{-1}$ during the 100th

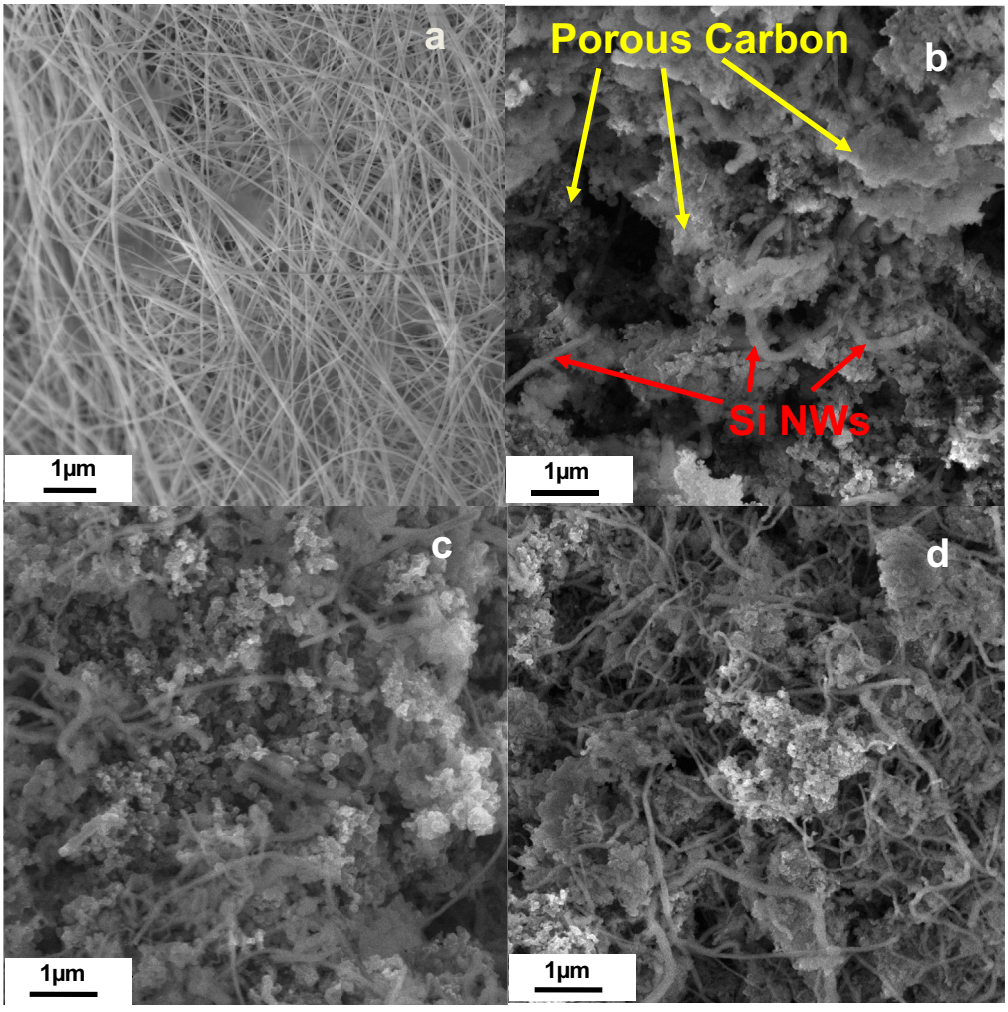


**Fig. 5.** SEM images of (a) pure Si nanowires and porous carbon loaded with (b) 54.5%, (c) 71.4% and (d) 80% of Si nanowires.

cycle. The low discharge capacities indicates that the massive volume change of the Si leads to lose of electronic contact with current collectors, which resulted in bad cycling performance although the first cycle capacity is almost reaching the theoretical capacity. The first discharge capacity of Si NWs/PC composites is lower than that of pure Si NWs and decreased with increasing amount of porous carbon that has a low specific capacity. However, the slope of the capacity fading of Si NWs/PC electrodes are lower than that of pure Si NWs, which means their cycling performance are better for samples with porous carbon than that of pure Si NWs. From the second cycle, the Si NWs/PC composites with 80% and 71.4% Si NWs show higher capacity than pure Si NWs, and their capacity decrease slowly with a gentle sloping line, and maintaining 1678 and 1390 mAh $g^{-1}$ during 100th cycle. Although the capacity for Si NWs/PC composite with 54.5% Si NWs is lower than the pure Si NWs at the second cycle, it is more stable and higher than that of pure Si NWs after 10 cycles, and maintains at 1188 mAh $g^{-1}$ during the 100th cycle. This performance is comparable to carbon coated Si NWs which shows 1110 mAh $g^{-1}$ after 40 cycles [6].The higher initial reversible capacities obtained in Si NWs/PC samples as compared to that of pure Si NWs were possibly due to the existence of porous carbon that served as conduction channels to facilitate the effective charge transfer between the Si nanocrystals and electrolytes. The stable cycling performance of the Si NWs/PC composite was attributed to the porous carbon in the hybrid samples that served as a highly conductive framework to maintain the electrical contact between the Si and the current collectors and absorption of volume changes of Si nanowries during lithiation/delithiation.

To further understand the electrochemical dynamic behaviors of pure Si NWs and Si NWs/PC composite electrodes, electrochemical impedance spectroscopy (EIS) measurements were performed

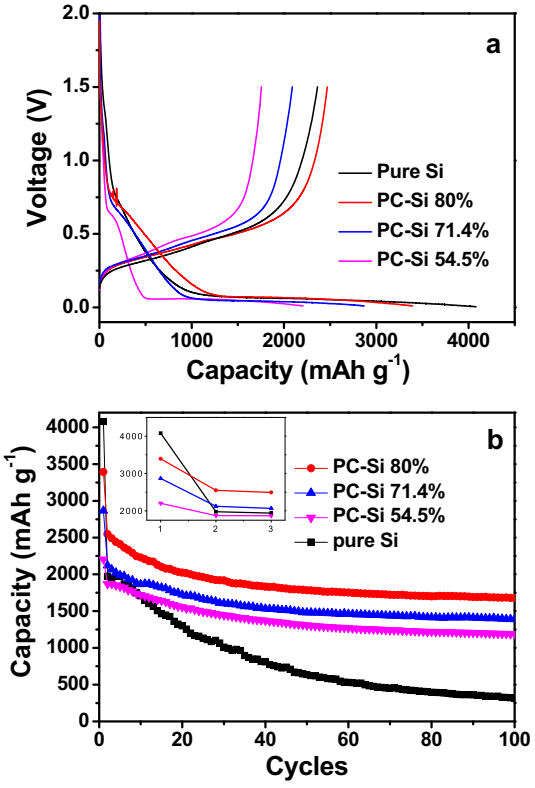


**Fig. 6.** (a) Initial voltage profiles and (b) Cycling performance of the Si NWs, porous carbon loaded with 54.5%, 71.4% and 80% of Si nanowires electrodes at a current density of 420 mA $g^{-1}$ (0.1C) between 0 and 1.5 V. Insert in (b): the capacity of first three cycles are omitted for clarify.

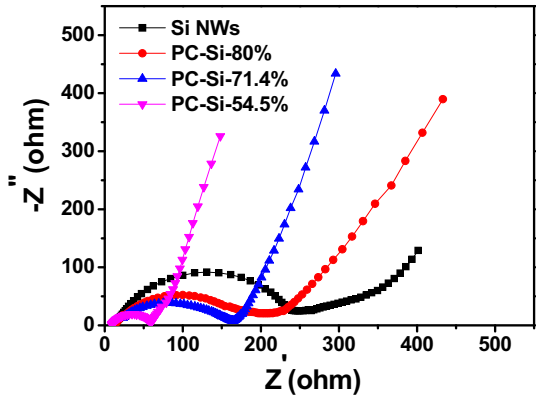


**Fig. 7.** EIS plots of electrodes made of the Si NWs, porous carbon loaded with 54.5%, 71.4%, and 80% of Si nanowires.

(Fig. 7). The cells were initially galvanostatical charged/discharged for three cycles to ensure the formation of stable SEI films and percolation of electrode materials by the electrolyte, and then AC impedance was measured at the fully charged state. As shown in Fig. 7, impedance spectra are composed of one semicircular arc at high-middle frequency region representing the charge-transfer process, followed by a straight line at low frequency region, corresponding to the diffusion of Li ions in the electrode materials [36]. Obviously, the semicircular arc of pure Si NWs is the largest, which indicates its highest charge transfer resistance. After incorporation with porous carbon, the charge transfer resistances are significantly decreased, especially for the sample with more carbon (*i.e.*, PC-Si 54.5%). This observation indicates that the introduction of porous carbon can enhance the electrochemical activities of Si NWs and facilitate the electron transport during the $Li^+$ insertion/extraction processes which are both favorable for improving the cycle performance and rate capability of Si NWs.

## 4. Conclusions

In summary, Si NWs/PC nanocomposites were successfully synthesized by using SFLS process. The porous carbon in these composite nanostructures was expected to facilitate the electron transportation, and absorb the volume changes of Si nanowires during the lithiation/delithiation processes. As a result, these Si NWs/PC electrodes exhibited lower charge transfer resistances, higher specific capacities and better charge-discharge cycling stabilities as anode materials for lithium ion batteries. At optimized condition, the Si nanowires (80%)/porous carbon electrode maintained reversible capacity of 1678 mAh $g^{-1}$ after 100 cycles at a current density of 420 mA $g^{-1}$, which was much better as compared to that of pure Si nanowires (316 mAh $g^{-1}$). Such synthesis approach can be promising steps for scalable production of Si NWs/carbon based nanocomposites with improved Li ion storage performance.

## Acknowledgment

The authors gratefully acknowledge AcRF Tier 1 RG 31/08 of MOE (Singapore), NRF2009EWT-CERP001-026 (Singapore), Singapore Ministry of Education (MOE2010-T2-1-017), A*STAR SERC grant 1021700144, Singapore MPA 23/04.15.03 grant, and Nanyang Technological University under the Undergraduate Research Experience on Campus (URECA) programme.

## References

[1] H.K. Song, K.T. Lee, M.G. Kim, L.F. Nazar, J. Cho, Adv. Funct. Mater. 20 (2010) 3818–3834.

[2] Y. Wang, G.Z. Cao, Adv. Mater. 20 (2008) 2251–2269.
[3] J.R. Szczech, S. Jin, Energy Environ. Sci. 4 (2011) 56–72.
[4] J.X. Zhu, T. Zhu, X.Z. Zhou, Y.Y. Zhang, X.W. Lou, X.D. Chen, H. Zhang, H.H. Hng, Q.Y. Yan, Nanoscale 3 (2011) 1084–1089.
[5] X.W. Guo, X.P. Fang, Y. Sun, L.Y. Shen, Z.X. Wang, L.Q. Chen, J. Power Sourc. 226 (2013) 75–81.
[6] C.K. Chan, R.N. Patel, M.J. O'Connell, B.A. Korgel, Y. Cui, ACS Nano 4 (2010) 1443–1450.
[7] S.Y. Chew, Z.P. Guo, J.Z. Wang, J. Chen, P. Munroe, S.H. Ng, L. Zhao, H.K. Liu, Electrochem. Commun. 9 (2007) 941–946.
[8] C.M. Park, J.H. Kim, H. Kim, H.J. Sohn, Chem. Soc. Rev. 39 (2010) 3115–3141.
[9] W. Wang, M.K. Datta, P.N. Kumta, J. Mater. Chem. 17 (2007) 3229–3237.
[10] C.K. Chan, H.L. Peng, G. Liu, K. McIlwrath, X.F. Zhang, R.A. Huggins, Y. Cui, Nat. Nanotechnol. 3 (2008) 31–35.
[11] S. Golmon, K. Maute, S.H. Lee, M.L. Dunn, Appl. Phys. Lett. 97 (2010).
[12] Z.Y. Lu, J.X. Zhu, D.H. Sim, W.W. Zhou, W.H. Ship, H.H. Hng, Q.Y. Yan, Chem. Mater. 23 (2011) 5293–5295.
[13] H. Ma, F.Y. Cheng, J. Chen, J.Z. Zhao, C.S. Li, Z.L. Tao, J. Liang, Adv. Mater. 19 (2007) 4067–4070.
[14] H.X. Chen, Z.X. Dong, Y.P. Fu, Y. Yang, J. Solid State Electrochem. 14 (2010) 1829–1834.
[15] L.F. Cui, R. Ruffo, C.K. Chan, H.L. Peng, Y. Cui, Nano Lett. 9 (2009) 491–495.
[16] M.H. Park, M.G. Kim, J. Joo, K. Kim, J. Kim, S. Ahn, Y. Cui, J. Cho, Nano Lett. 9 (2009) 3844–3847.
[17] H.X. Chen, Y. Xiao, L. Wang, Y. Yang, J. Power Sourc. 196 (2011) 6657–6662.
[18] X.H. Rui, D.H. Sim, C. Xu, W.L. Liu, H.T. Tan, K.M. Wong, H.H. Hng, T.M. Lim, Q.Y. Yan, RSC Adv. 2 (2012) 1174–1180.
[19] X.H. Rui, J.X. Zhu, W.L. Liu, H.T. Tan, D.H. Sim, C. Xu, H. Zhang, J. Ma, H.H. Hng, T.M. Lim, Q.Y. Yan, RSC Adv. 1 (2011) 117–122.
[20] P.C. Chen, J. Xu, H.T. Chen, C.W. Zhou, Nano Res. 4 (2011) 290–296.
[21] T. Hasegawa, S.R. Mukai, Y. Shirato, H. Tamon, Carbon 42 (2004) 2573–2579.
[22] S.H. Ng, J. Wang, D. Wexler, S.Y. Chew, H.K. Liu, J. Phys. Chem. C 111 (2007) 11131–11138.
[23] S.H. Ng, J.Z. Wang, D. Wexler, K. Konstantinov, Z.P. Guo, H.K. Liu, Angew. Chem. Int. Edit 45 (2006) 6896–6899.
[24] J.P. Rong, C. Masarapu, J. Ni, Z.J. Zhang, B.Q. Wei, ACS Nano 4 (2010) 4683–4690.
[25] L.W. Su, Z. Zhou, M.M. Ren, Chem. Commun. 46 (2010) 2590–2592.
[26] W. Wang, P.N. Kumta, ACS Nano 4 (2010) 2233–2241.
[27] J.K. Lee, K.B. Smith, C.M. Hayner, H.H. Kung, Chem. Commun. 46 (2010) 2025–2027.
[28] Y.J. Cho, H.S. Kim, H. Im, Y. Myung, G.B. Jung, C.W. Lee, J. Park, M.H. Park, J. Cho, H.S. Kang, J. Phys. Chem. C 115 (2011) 9451–9457.
[29] X.S. Zhou, Y.X. Yin, L.J. Wan, Y.G. Guo, Chem. Commun. 48 (2012) 2198–2200.
[30] A. Magasinski, P. Dixon, B. Hertzberg, A. Kvit, J. Ayala, G. Yushin, Nat. Mater. 9 (2010) 353–358.
[31] X.M. Lu, T. Hanrath, K.P. Johnston, B.A. Korgel, Nano Lett. 3 (2003) 93–99.
[32] X.L. Wang, W.Q. Han, ACS Appl. Mater. Inter. 2 (2010) 3709–3713.
[33] T.D. Hatchard, J.R. Dahn, J. Electrochem. Soc. 151 (2004) A838–A842.
[34] Y. Yu, L. Gu, C.B. Zhu, S. Tsukimoto, P.A. van Aken, J. Maier Adv. Mater. 22 (2010) 2247–2250.
[35] C.K. Chan, R. Ruffo, S.S. Hong, Y. Cui, J. Power Sourc. 189 (2009) 1132–1140.
[36] X.H. Rui, X.X. Zhao, Z.Y. Lu, H.T. Tan, D.H. Sim, H.H. Hng, R. Yazami, T.M. Lim, Q.Y. Yan, ACS Nano 7 (2013) 5637–5646.